

Original Research

Prognostic Cell Death Index for Lung Adenocarcinoma: A Comprehensive Transcriptome-Based Analysis of Twelve Programmed Cell Death Pattern Genes

Funan Chen¹, Jun Ma¹, Shuqiao Hu¹, Canxing Wu¹, Shanshan Chen¹, Jiehuan Lin^{1,*}¹Department of Thoracic and Cardiac Surgery, Longyan First Affiliated Hospital of Fujian Medical University, 364000 Longyan, Fujian, China*Correspondence: Jiehuan_Lin@outlook.com (Jiehuan Lin)

Academic Editor: Eun Sook Hwang

Submitted: 23 September 2023 Revised: 14 January 2024 Accepted: 6 February 2024 Published: 1 April 2024

Abstract

Objective: Lung adenocarcinoma (LUAD) is a prominent contributor to global cancer mortality, characterized by constrained prognosis. This study aimed to develop a novel prognostic indicator, the Cell Death Index (CDI), utilizing twelve programmed cell death (PCD) pattern genes, to predict the immune infiltration and prognosis in LUAD patients. **Methods:** We collected PCD-related genes and identified prognostic PCD genes in the Cancer Genome Atlas (TCGA)-LUAD dataset, and made rigorous validation in the Clinical Proteomic Tumor Analysis Consortium (CPTAC)-LUAD cohorts. CDI was calculated using a multivariable Cox regression model. Functional enrichment and tumor microenvironment were evaluated. Drug sensitivity prediction and nomogram development were performed to assess CDI's potential value. **Results:** The results revealed 10 PCD genes (*ERO1A*, *CDK5R1*, *TRIM6*, *DNASE2B*, *ITPRIP*, *MRGPRX2*, *FGA*, *NDUFA13*, *NLRP2*, and *CD68*) significantly associated with LUAD prognosis. The CDI was constructed and showed high accuracy in predicting patient survival with C-index values of 0.801 and 0.794 in the prognosis cohort and validation cohort, respectively. CDI is also indicative of variations in biological functions, tumor microenvironment, and immune cell infiltration including neutrophils, activated mast cells, activated dendritic cells, M0 macrophages, resting natural killer cells, $\gamma\delta$ T cells, and activated memory CD4⁺T cells. Furthermore, drug sensitivity analysis indicated potential targeted strategies. **Conclusions:** The CDI, based on PCD genes, serves as a robust prognostic tool for LUAD, offering profound insights into tumor biology, immune response, and personalized treatment strategies. This study underscores the pivotal role of PCD mechanisms in LUAD pathogenesis and identifies potential therapeutic targets.

Keywords: lung adenocarcinoma; prognostic indicator; programmed cell death genes; immune infiltration; personalized treatment strategies

1. Introduction

Lung cancer is the leading cause of tumor burden worldwide, based on the GLOBOCAN 2020 estimates [1]. The pathogenic mechanism of lung cancer has not been thoroughly elucidated [2]. The lung cancer-related mortality accounts for approximately 20% of the total cancer deaths worldwide, with a total of 1.59 million deaths in 2012 [3]. Lung cancer has been historically classified into small cell lung cancer (SCLC) and non-small cell lung cancer (NSCLC), with the latter constituting three-quarter of all lung cancer [4]. NSCLC is classified as adenocarcinoma (60%), squamous cell carcinoma (30%) and other rare subtypes (10%). Lung adenocarcinoma (LUAD) continues to be the predominant histological subtype of NSCLC and is associated with an overall 5-year survival rate of less than 19.4% [5]. In light of the poor prognosis observed in LUAD, there exists an imperative unmet need to delve into novel therapeutic targets aimed at enhancing the prognosis of LUAD. The development of efficient models is also pivotal to render immunotherapy more practicable.

Programmed cell death (PCD), recognized as an active, programmed procedure of autonomous cellular dis-

mantling, is characterized by the absence of cytoplasmic content release to the extracellular milieu [6,7]. In recent decades, several types of PCD have been found and defined [8]. PCD consists of several types of cell death such as apoptosis, necroptosis, ferroptosis, parthanatos, netotic cell death, pyroptosis, entotic cell death, autophagy-dependent cell death, oxeiptosis, lysosome-dependent cell death, and alkaliptosis [9]. Advancements in research have revealed that various forms of PCD, including apoptosis, pyroptosis, ferroptosis, and lysosome-dependent cell death, play significant roles in cancer pathogenesis. These mechanisms hold promise as novel targets for prospective anti-cancer therapies. For instance, some molecules such as circRNAs can regulate the process of pyroptosis via directly binding to miRNA as a sponge, thus releasing the inhibition of miRNA on PIF1, which finally mediates DNA damage and promotes inflammasome activation in lung adenocarcinoma [10]. Due to the advances in understanding the role of PCD, increasing number of related remedies were explored and applied in disease management.

Currently, evidence suggested that PCD makes a remarkable difference in the progression and invasion of malignant cancers. Cancer cells would not be able to develop



further without resisting multiple types of PCD [11]. However, a thorough investigation of the association through PCD and LUAD remains unclear, and the specific role of PCD in LUAD has been less understood. Additionally, the recent development in array-based technologies enable us to thoroughly explore the survival-related genes for prognosis to identify potential targets [12]. Thus, in the present research, we aim to construct a novel predictor, namely cell death index (CDI), to evaluate the effectiveness of immune infiltration and survival with respect to LUAD, and to provide theoretical basis for the decision of tailored treatment strategy for LUAD individuals.

2. Methods

2.1 Study Workflow

A total of 1466 genes (**Supplementary Table 1**) that are associated with twelve PCD procedures were collected from available gene sets, recent papers, and manual search [9]. Firstly, the PCD genes with prognostic value were identified in the Cancer Genome Atlas (TCGA)-LUAD cohort (prognosis cohort). The prognostic CDI was constructed and then validated in the Clinical Proteomic Tumor Analysis Consortium (CPTAC)-LUAD cohort (validation cohort). The correlation of CDI with clinical outcomes, functional enrichment, tumor microenvironment and drug sensitivity prediction was further investigated. The workflow diagram of this research is delineated in Fig. 1.

2.2 PCD Genes Expression and Related Functions

Raw transcriptome counts data from LUAD and normal lung tissues were subjected to comparison within the TCGA database. The DESeq2 package was used to identify differentially expressed genes (DEGs), with the criterion criteria set at adjusted $p < 0.05$ and $|\log_2 \text{fold change (FC)}| > 1$. The biological function enrichment of these DEGs was elucidated through the Database for Annotation, Visualization and Integrated Discovery (DAVID).

2.3 Construction of the Prognostic CDI

To pinpoint the PCD genes with significant implications for the prognosis of LUAD, a series of analyses including univariate Cox regression, Least Absolute Shrinkage and Selection Operator (LASSO) Cox regression and multivariate Cox regression were executed. The ultimate prognostic CDI of each patient was calculated by the sum up the product of risk coefficient and the expression of each prognostic PCD gene. Subsequent exploration delved into the association of CDI with clinical status, encompassing survival, tumor stage, etc.

2.4 Functional Difference in High- and Low-CDI Patients

LUAD patients were stratified into high- and low-CDI groups based on the median CDI score of the TCGA-LUAD cohort. Gene set variation analysis (GSVA) was utilized

to explore the altered biological signaling pathways among patients with high- and low-CDI through the R packages GSVA.

2.5 Evaluation of Independent Prognostic Performance of CDI

The independent prognostic efficacy of CDI score was appraised in TCGA-LUAD cohort and subsequently validated in CPTAC-LUAD cohort. The Kaplan-Meier curves depicting the high- and low-CDI groups of LUAD patients were constructed and compared. Employing the CDI score as the predictive variable, Receiver Operating Characteristic (ROC) curves were delineated at 1-, 3- and 5-year, with the area under the receiver operating characteristic curve (AUC) calculated using the timeROC R package. Calibration curves and dot plots were generated to generated the congruence of CDI-predicted survival and actual survival.

2.6 Unsupervised Clustering

Based on the expression matrix of CDI genes, the ConsensusClusterPlus package was used to investigate the unidentified subtypes of LUAD. The parameter of consensus clustering was chosen as follows: maxK = 8, clusterAlg = hc and distance = pearson. The parameter k means that each sample is partitioned into up to k cluster by a specified clustering algorithm of agglomerative hierarchical clustering.

2.7 Establishment of the Nomogram

To verify the independent prognostic significance of CDI, univariate Cox regression and stepwise multivariate Cox regression were conducted, incorporating CDI score along with clinical parameters. To further developed a prognostic nomogram, the stepwise regression was conducted to select the final model factors. The predictive performance of the nomogram was evaluated using the Kaplan-Meier curve, AUC and calibration analysis as described above.

2.8 Relationship between CDI and Tumor Microenvironment

The mRNA levels of 70 immunomodulators which were involved in the functions including antigen presentation, cell adhesion, coinhibitor, costimulator, ligand, receptor, etc., were analysed to identify their correlation with CDI level. Then, we used CIBERSORT (Cell-type Identification by Estimating Relative Subsets of RNA Transcripts) to measure the infiltration of 22 types of immune cells in the LUAD tumors of the high- and low-CDI groups. CIBERSORT is a computational method for estimating immune cell composition in complex tissues base on their gene expression profiles.

2.9 Prediction of Drug Sensitivities

Inhibitory concentration (IC₅₀) of nearly two hundred common anti-tumor agents for each patient were predicted

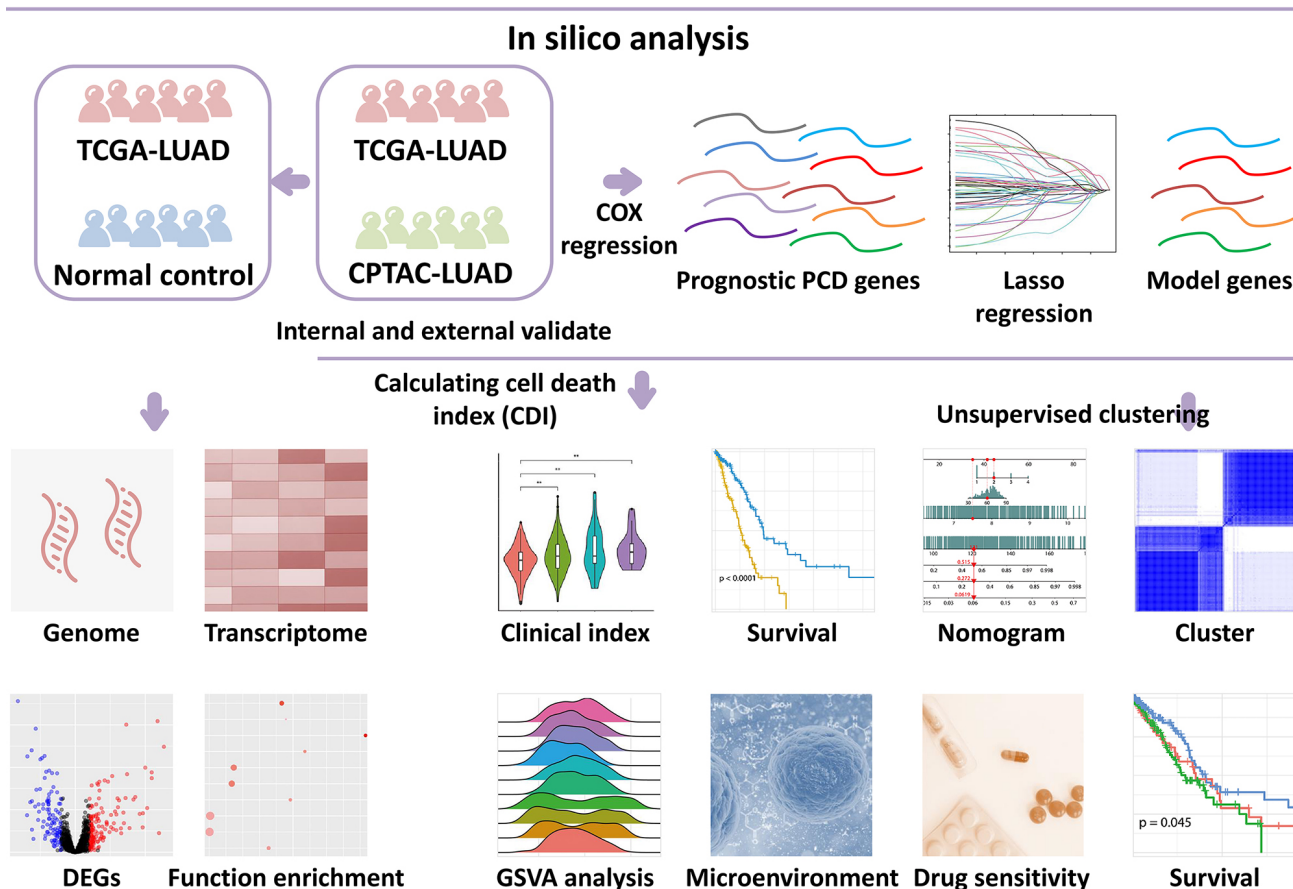
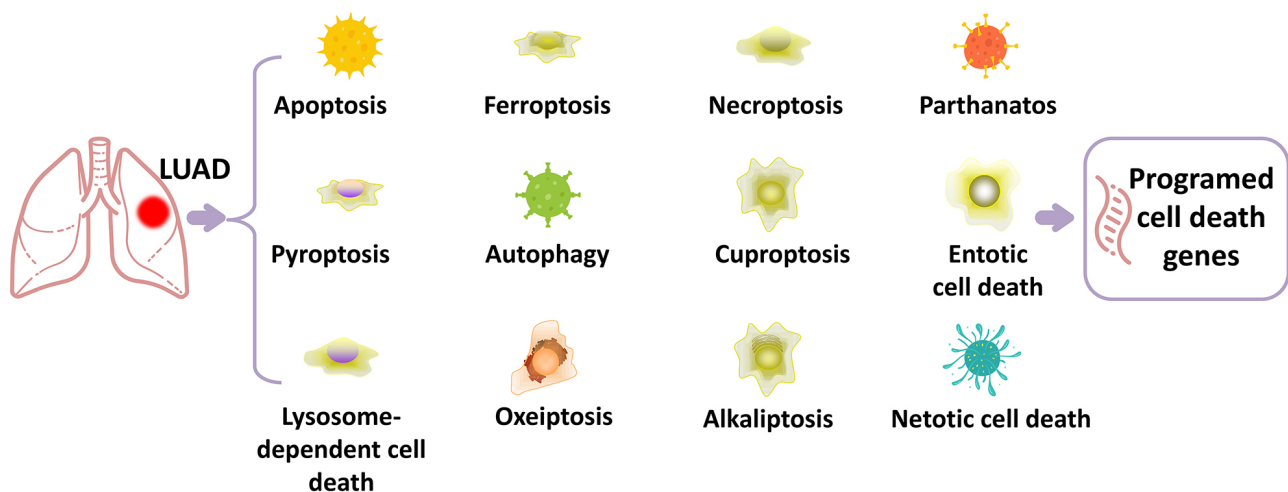


Fig. 1. Overview of the main workflow of this study. LUAD, lung adenocarcinoma; TCGA, the Cancer Genome Atlas; CPTAC, the Clinical Proteomic Tumor Analysis Consortium; PCD, programmed cell death; DEGs, differentially expressed genes; GSVA, gene set variation analysis.

by using the oncoPredict package in R. To assess the potential response to immunotherapy, Tumor Immune Dysfunction and Exclusion (TIDE) algorithm was employed between high- and low-CDI groups.

2.10 Statistical Analysis

R software (v.4.3.0, <https://www.r-project.org/>) was used to perform all statistical analysis. Cumulative survival curve was presented by Kaplan-Meier plot and the differences of survival were evaluated using the log-rank test. p value less than 0.05 was considered as statistical significance.

3. Results

3.1 Expression Profile of PCD Genes in LUAD

In the prognosis cohort, a total of 236 DEGs encompassing 136 up-regulated genes and 100 down-regulated genes were delineated (Fig. 2A and **Supplementary Table 2**). The expression heatmap of these DEGs showed pronounced disparities between LUAD and normal lung tissues (Fig. 2B). To elucidate the primary functions associated with these DEGs, Gene Ontology (GO) and Kyoto Encyclopedia of Genes and Genomes (KEGG) enrichment analysis were performed (Fig. 2C–F). The results indicated that these PCD DEGs are intricately linked to diverse functional pathways, including apoptotic process, inflammatory response, pathways in cancer and others.

3.2 Identification of a Prognosis-Related PCD Gene Signature (CDI) for LUAD

Univariate COX regression analysis identified 49 PCD genes that were significantly linked to the survival of LUAD patients in the prognosis cohort with p value < 0.05 (**Supplementary Table 3**). Using the LASSO COX regression, the collinearity between PCD genes as well as those with less pronounced survival significance were eliminated (Fig. 3A,B), and 15 genes were further selected. These 15 genes were then integrated into a multivariable COX regression model, and a stepwise selection analysis were performed. Consequently, the ultimate prognostic model comprised 10 PCD genes, namely *ERO1A*, *CDK5R1*, *TRIM6*, *DNASE2B*, *ITPRIP*, *MRGPRX2*, *FGA*, *NDUFA13*, *NLRP2*, and *CD68* (Fig. 3C). The CDI for each patient can be computed based on the expression level of these 10 genes using the following formula: $CDI = 0.2052 \times ERO1A + 0.2821 \times CDK5R1 + 0.3238 \times TRIM6 + (-0.1625) \times DNASE2B + (0.3568) \times ITPRIP + 0.3277 \times MRGPRX2 + 0.0672 \times FGA + (-0.2602) \times NDUFA13 + (-0.1133) \times NLRP2 + (-0.4214) \times CD68$.

The relationship of CDI with clinical features were depicted in Fig. 3D. LUAD patients in the prognosis cohort who experienced mortality during follow-up demonstrated a notably higher CDI score. Furthermore, an observable inclination towards elevated CDI was noted in the context of more advanced tumor stages, encompassing American Joint Committee on Cancer (AJCC) stage, T stage, and N stage.

In furthering our comprehension of the distinctions in biological function status between high- and low-CDI groups, KEGG pathways analysis demonstrated that the cell cycle, P53 signaling pathway and several cancer pathways were notably prominent (Fig. 3E,F).

3.3 Internal and External Validation of the CDI

Employing the CDI as a prognostic factor, the predictive performance was evaluated in prognosis cohort and validation cohort, respectively. LUAD patients with high-CDI showed worse survival probability in both cohorts (Fig. 4A,B). The AUC values of CDI in the prognosis co-

hort at 1-, 3- and 5-year of follow-up were 0.784, 0.796 and 0.805, respectively, with the C-index value of 0.801 (Fig. 4C). The CDI also demonstrated commendable performance in the validation cohort with 1-, 3- and 5-year AUC values of 0.803, 0.787 and 0.778, respectively, as well as the C-index value of 0.794 (Fig. 4C). The calibration analysis of CDI in predicting the survival also exhibited highly favorable fitting with the actual survival outcomes in both LUAD cohorts (Fig. 4D,E).

3.4 Unsupervised Clustering Based on PCD Signature

To investigate the unidentified subsets of LUAD, 10 PCD signature genes were utilized to conduct the consensus clustering procedure. According to the consensus index and Cumulative Distribution Function (CDF) curve, it was observed that the most significant differences among subsets were evident when $k = 3$ (Fig. 5A–C). Subsequently, there was a significant difference in survival among the subsets of LUAD patients (Fig. 5D). The distribution of survival and CDI risk groups revealed that cluster 3 was associated with a lower CDI and better survival outcome (Fig. 5E).

3.5 Construction and Evaluation of the Prognostic Nomogram

COX regression analysis showed that CDI is a significant risk factor for LUAD survival independent of the clinical factors including age, sex, stages of tumor (T), lymph node (N), metastases (M) and the AJCC stage (Fig. 6A,B). When adjusted for potential confounding variables which were non-significant in the multivariable COX model such as age, sex, etc., the hazard ratio for CDI was 2.655 (95% Confidence Interval (CI), 2.009–3.508, $p < 0.001$). A prognostic nomogram model was established after multivariate COX regression and stepwise selection. AJCC stage, age and CDI were finally used for construction of the nomogram (Fig. 6C). The red lines, arrows and dots were plotted on the nomogram to show an example of how to use the nomogram. For a LUAD patient of 60 years old, stage II and with CDI score of 7.5, he gets a total risk score of 121 points which indicates that the 1-, 3- and 5-year death probability were 0.0619, 0.272 and 0.515, respectively. The Kaplan-Meier curves of the nomogram-predicted high- and low-points groups showed very obvious separation in both cohorts (Fig. 6D). The AUC values of 1-, 3- and 5-year ROC curves were all beyond 0.75, suggesting that the nomogram had a relatively high accuracy (Fig. 6E). Besides, the calibration curves also indicate favorable fitting of the predicted survival with actual survival outcomes (Fig. 6F).

3.6 Dissection of Tumor Microenvironment Based on CDI

The correlation analysis of CDI with the expression of immune-related genes suggested that higher CDI level might had lower antigen presentation, cell adhesion and stronger coinhibitor, indicating a relatively

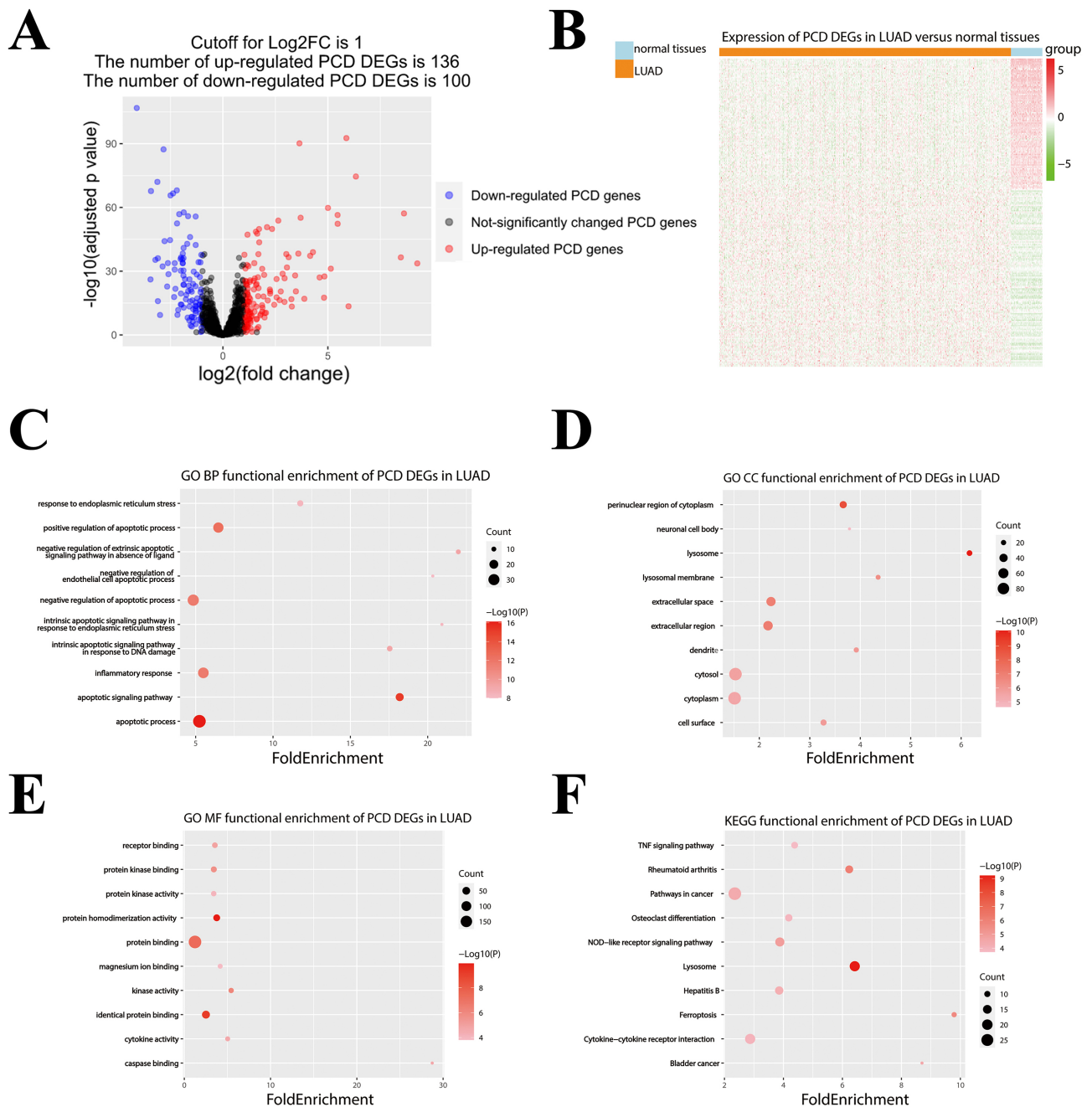


Fig. 2. Exploration of Differentially Expressed Genes (DEGs) in PCD in LUAD. (A) Volcano plot depicting Log fold change (FC) changes and p -values of DEGs in PCD relative to normal controls in LUAD. (B) Heatmap showing the expression levels of DEGs in PCD in both LUAD and normal controls. (C–F) Representation of functional enrichment pathways for these DEGs in terms of gene ontology-biological process (GO BP), cellular component (GO CC), molecular function (GO MF), and Kyoto Encyclopedia of Genes and Genomes (KEGG), respectively.

immuno-tolerant microenvironment in these LUAD tissues (Fig. 7A). The estimated proportion of immune cells in the tumor microenvironment was also calculated and shown in Fig. 7B. Elevated CDI score was correlated with marked increase in the infiltration of neutrophils, activated mast cells, activated dendritic cells, M0 macrophages, resting natural killer (NK) cells, $\gamma\delta$ T cells, and activated memory CD4⁺T

cells. Conversely, there was a reduction in the infiltration of resting mast cells, resting dendritic cells, monocytes, and activated NK cells (Fig. 7C,D).

3.7 Efficacy of CDI in Evaluating Treatment Sensitivity

To investigate the correlation between the CDI score and treatment sensitivity, we obtained IC50 values of each

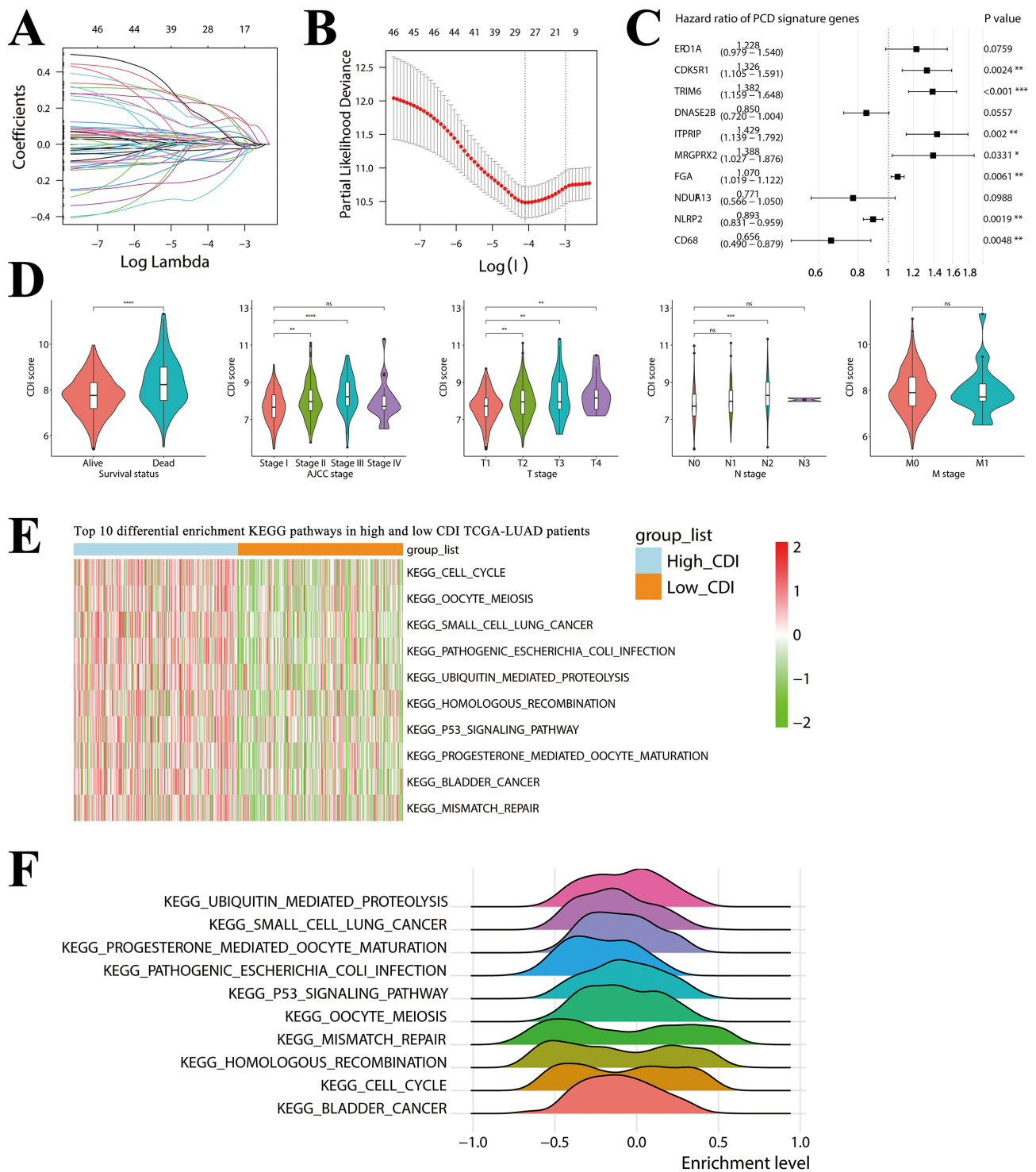


Fig. 3. Establishment of cell death index (CDI). (A,B) Illustration of the Least Absolute Shrinkage and Selection Operator (LASSO) regression process for penalty coefficients, resulting in the inclusion of 10 genes for modeling. (C) Display of hazard ratio values, 95% Confidence Interval (CI), and p -values for the 10 genes in the CDI model. (D) Association between CDI scores in LUAD patients and clinical indicators. (E,F) Differentiation of high and low CDI groups in LUAD patients based on CDI levels, presented as heatmap and ridge plot, highlighting the top 10 significantly enriched KEGG pathways for each group. *, $p < 0.05$; **, $p < 0.01$; ***, $p < 0.001$; ****, $p < 0.0001$; ns, non-significant.

agent in LUAD tissues to identify those showing significant differences. The top 20 drugs with the most significant cor-

relation of IC50 value with CDI score were recognized. As depicted in Fig. 8A, several commonly used chemothera-

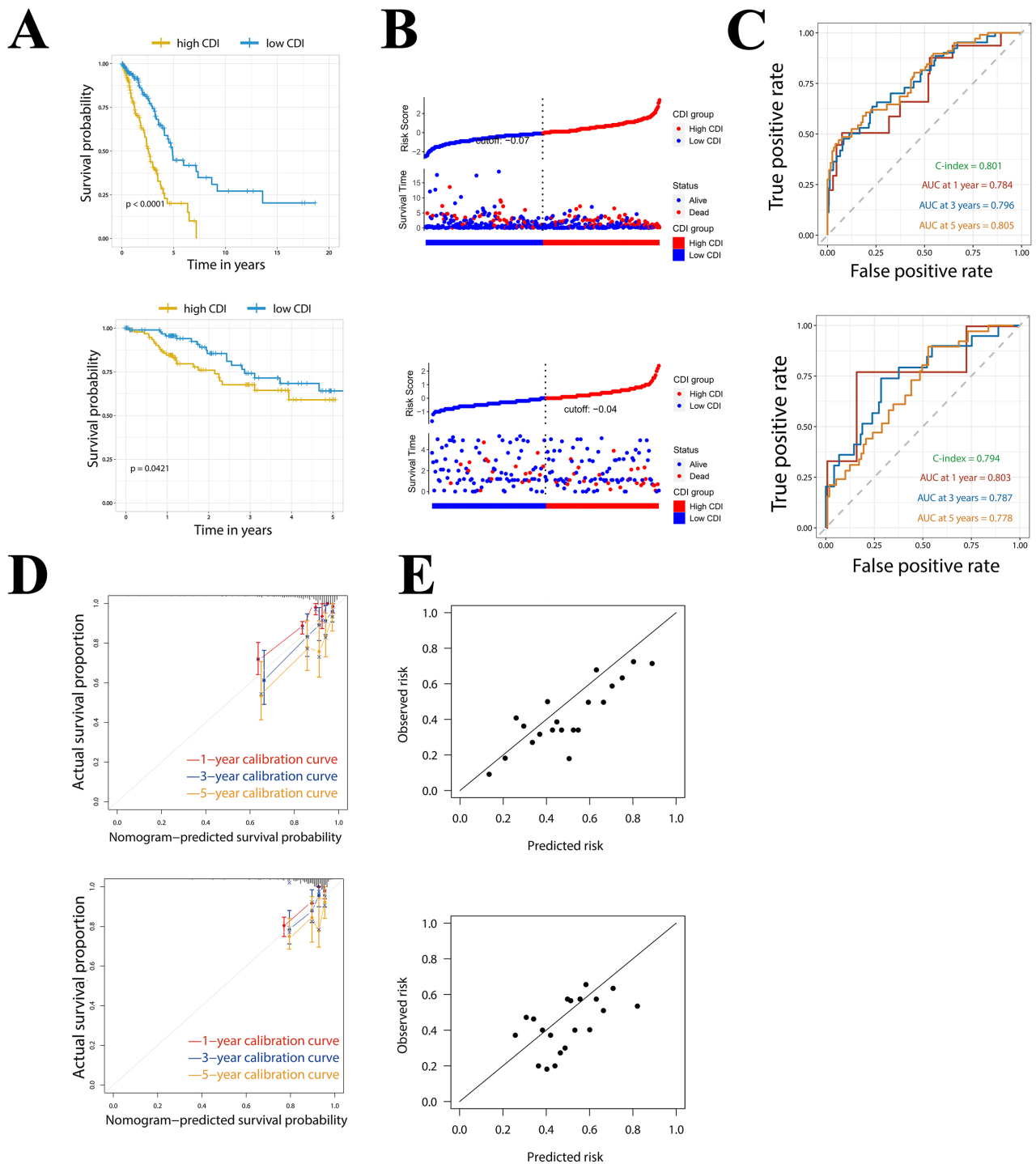


Fig. 4. Evaluation of the Prognostic Value of CDI. (A) Survival Kaplan-Meier (KM) curves for high and low CDI groups in LUAD patients from both TCGA and CPTAC datasets. (B) Correlation between individual patient survival risk and outcomes in high and low CDI groups from TCGA and CPTAC datasets. (C) Receiver Operating Characteristic (ROC) curves and area under the curve (AUC) values for CDI as a prognostic indicator in 1/3/5 years for LUAD patients in TCGA and CPTAC datasets. (D) Calibration curves for CDI as a prognostic indicator in 1/3/5 years for LUAD patients in TCGA and CPTAC datasets. (E) Calibration scatter plots for CDI as a prognostic indicator in 1/3/5 years for LUAD patients in TCGA and CPTAC datasets.

peutic drugs, such as cisplatin and targeting drugs, including osimertinib in NSCLC, were found to be highly associated with CDI score. Notably, patients with lower CDI scores appeared to be resistant to traditional chemothera-

peutic drugs such as cisplatin, docetaxel and gemcitabine (with higher IC50), but sensitive to the recent developed targeting drug osimertinib (Fig. 8B).

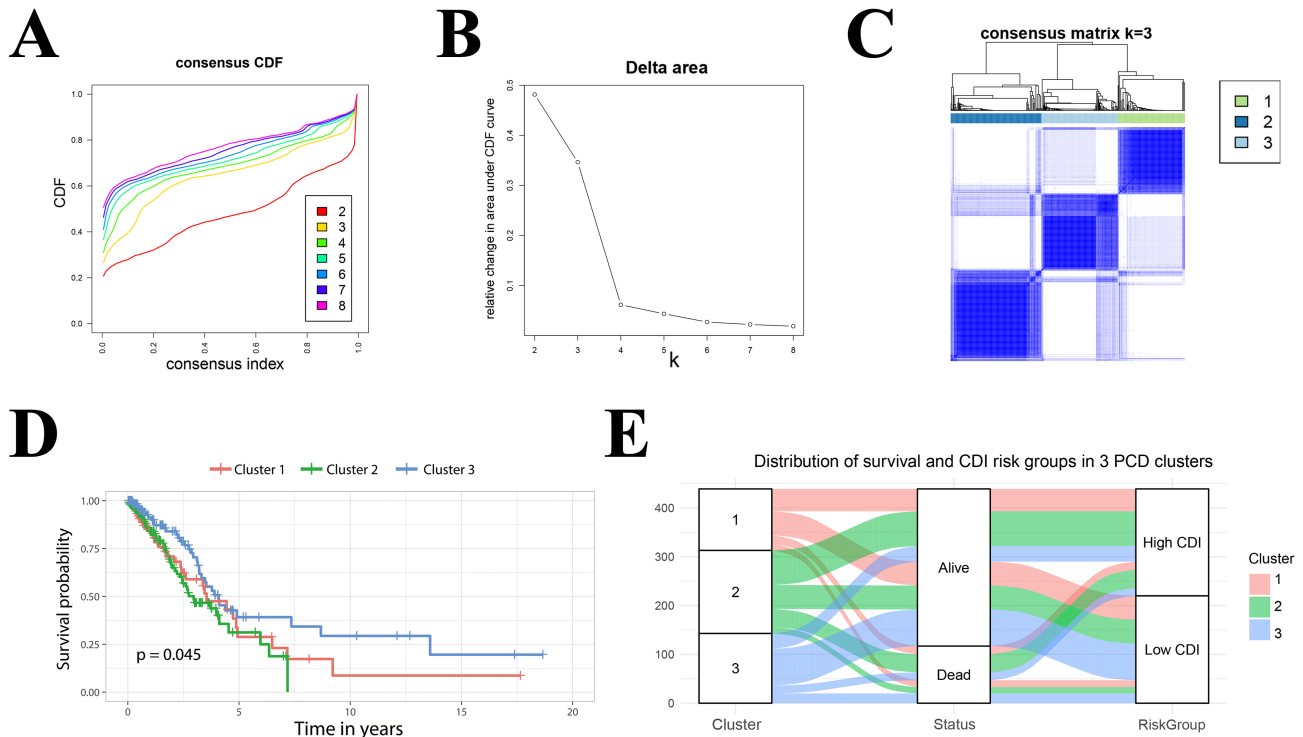


Fig. 5. Unsupervised Clustering Analysis Based on CDI Genes. (A–C) Clustering analysis process demonstrating three distinct patient clusters. (D) Survival KM curves for the three patient clusters. (E) Scatter plot showing the distribution of CDI levels and survival outcomes for patients in the three clusters. CDF, Cumulative Distribution Function.

Regarding immunotherapy prediction (Fig. 8C,D), CDI showed no significant difference in relation to the TIDE score. However, patients with higher CDI possessed elevated exclusion score and dysfunction score, suggesting a positive association between CDI and T cell immune exclusion, and a negative association with T cell function.

4. Discussion

This investigation marks a groundbreaking effort, being the first to meticulously probe the twelve PCD patterns within TCGA-LUAD patients. We devised a prognostic CDI and meticulously validated its reliability in an external cohort. The nomogram based on CDI and clinical parameters was constructed, revealing a highly promising prognostic utility. Additionally, the patients stratified into high- and low-CDI groups exhibited notable diversity in survival, biological functions, tumor environment, immune infiltration and drug resistance profiles.

Programmed cell death encompasses sophisticated modulation and intricately associated with complicated mechanisms. In recent decades, emerging evidence suggested that PCD is involved in many biological processes associated with the malignant behaviors of tumors [13–15]. Based on the capability to promote adaptive immune reaction or not, PCD can be classified as immunogenic and tolerogenic cell deaths [16]. Immunogenic PCD serves as an alert to the neighboring immune components of poten-

tial threat by releasing the cellular contents such as pro-inflammatory cytokines and damage-associated molecular patterns (DAMPs). These products can be identified by the Pattern Recognition Receptors (PRRs) present on innate immune cells, subsequently triggering immune reactions. On the contrary, tolerogenic PCD such as apoptosis, preserves the integrity of the cell membrane without releasing cellular components, thus resulting in a “quiet” clearance by the phagocytes with no further inflammatory response triggered [17]. Therefore, the PCD and related genes in tumors is a double-edged sword with both oncogenic and anti-tumor potentials.

A total of ten PCD genes were included in the prognostic model. These genes were attributed to apoptosis (*ERO1A*, *ITPR1P*, *FGA* and *NDUFA13*), autophagy (*CDK5R1* and *TRIM6*), lysosome-dependent cell death (*DNASE2B*, *MRGPRX2* and *CD68*) and pyroptosis (*NLRP2*), which might be more related with the prognosis of LUAD as compared with other types of PCD. *ERO1A* primarily promotes apoptosis by mediating endoplasmic reticulum stress. Through the *ERO1A*-IP3R pathway, it can activate IP3R, thereby triggering IP3-induced calcium release and consequently mediating calcium-dependent apoptosis [18]. Apoptosis is an early recognized non-immunogenic type of PCD [19], which is precisely encoded by the sequential cleavages of caspases [17]. The preponderance of model genes (three out of four) implicated in

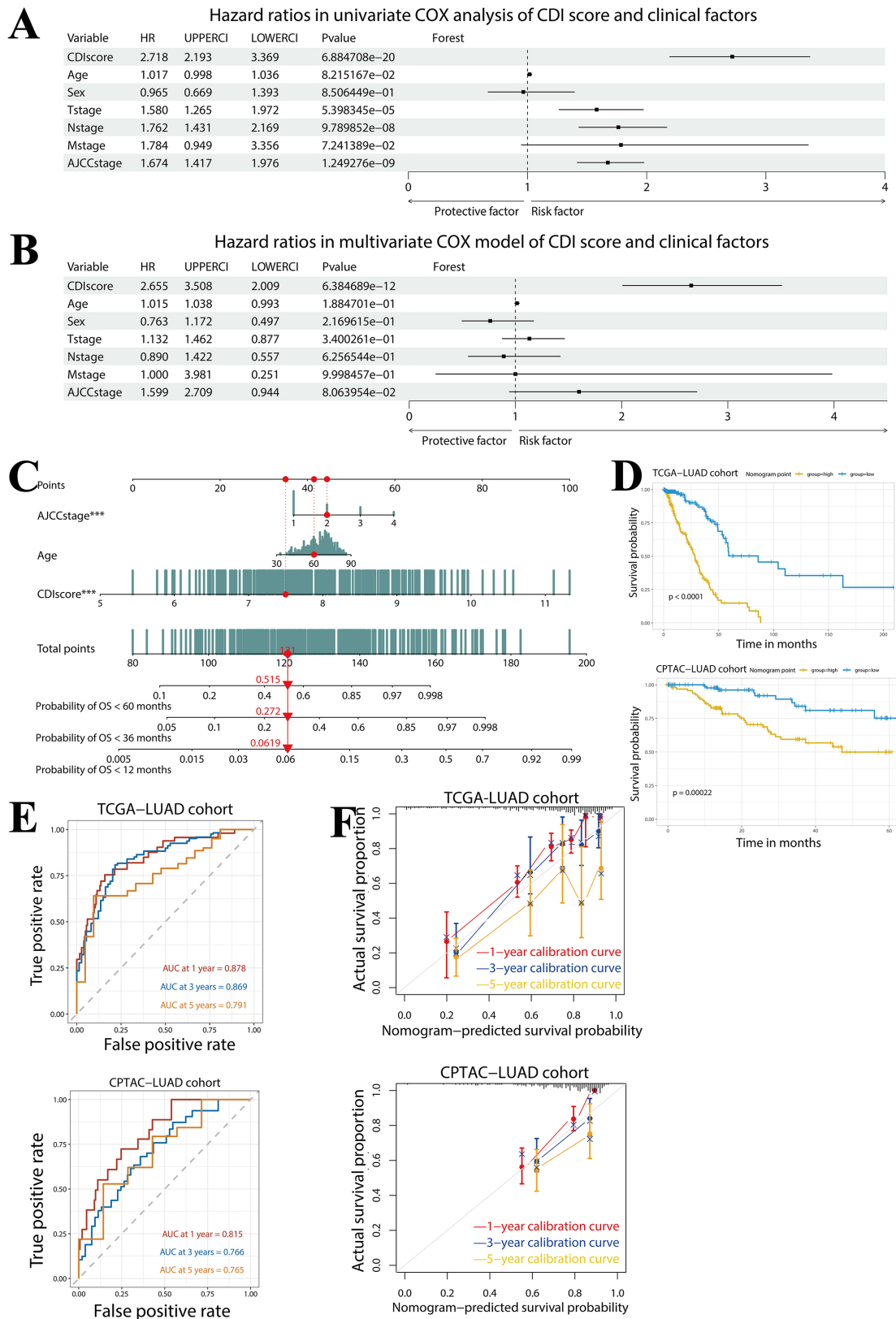


Fig. 6. Construction of Nomogram Based on CDI. (A,B) Forest plots displaying HR values, 95% CI, and p -values for CDI in single-factor Cox analysis and multi-factor Cox analysis, respectively. (C) Nomogram based on AJCC, age, and CDI, explaining how to predict a patient's 1/3/5-year survival probability. (D) KM curves for high-risk and low-risk groups predicted by nomogram for TCGA and CPTAC datasets. (E) ROC curves for 1/3/5-year survival prediction based on nomogram for TCGA and CPTAC datasets. (F) Calibration curves for 1/3/5-year survival prediction based on nomogram for TCGA and CPTAC datasets. HR, hazard ratio.

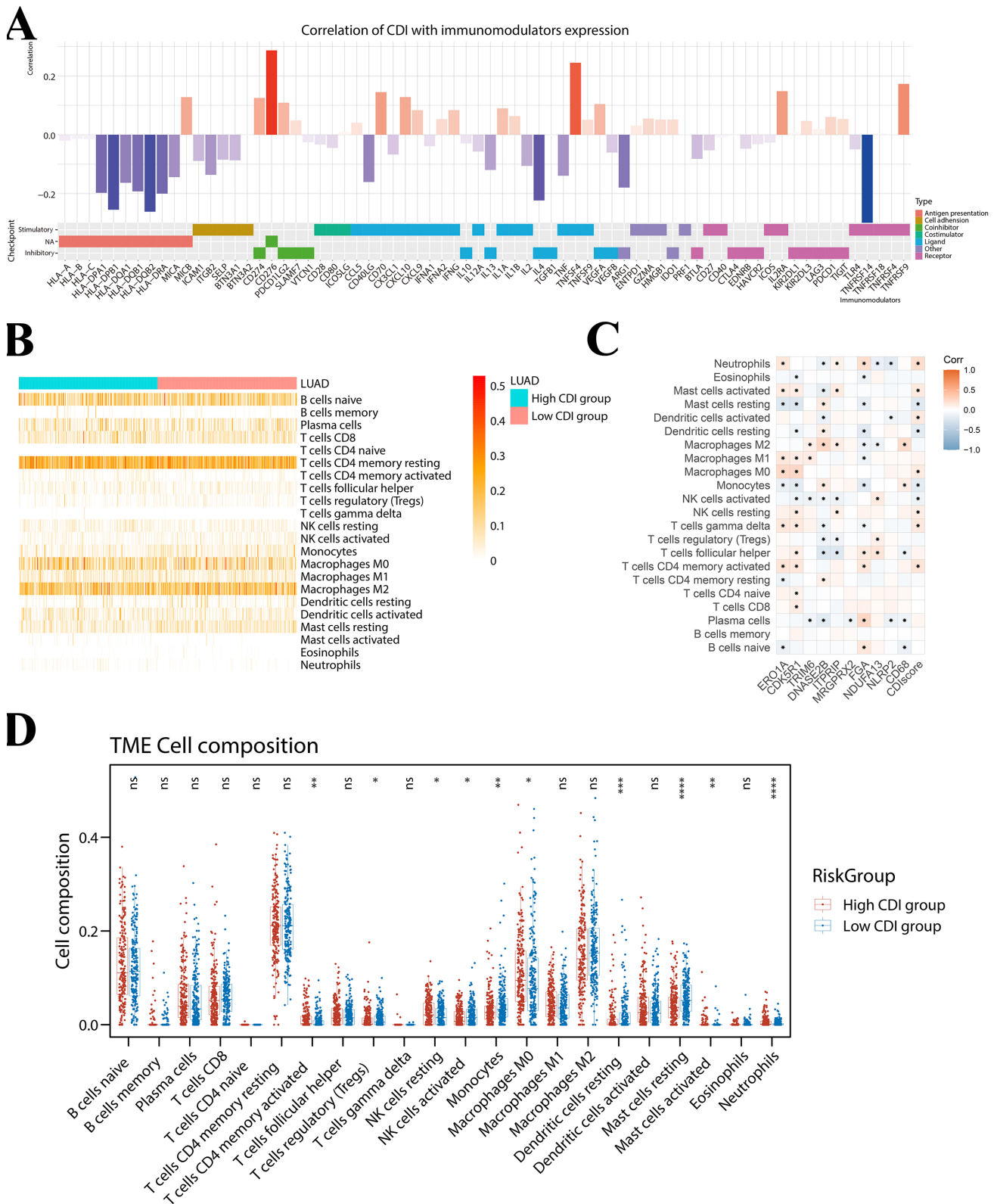


Fig. 7. Assessment of CDI-Related Immune Microenvironment. (A) Bar chart illustrating the correlation between CDI and various immune regulatory genes in LUAD patients from TCGA, with panel descriptions of each immune regulatory gene's properties and type. (B) Heatmap displaying the proportion levels of 22 immune cells in each LUAD patient from TCGA, stratified into high and low CDI groups. (C) Heatmap further showing the correlation between 22 immune cells, CDI, and the 10 CDI modeling genes, with asterisks indicating statistically significant correlations ($p < 0.05$). (D) Box plots summarizing the average levels and differences in 22 immune cells between high CDI and low CDI groups. *, $p < 0.05$; **, $p < 0.01$; ***, $p < 0.001$; ****, $p < 0.0001$; ns, non-significant.

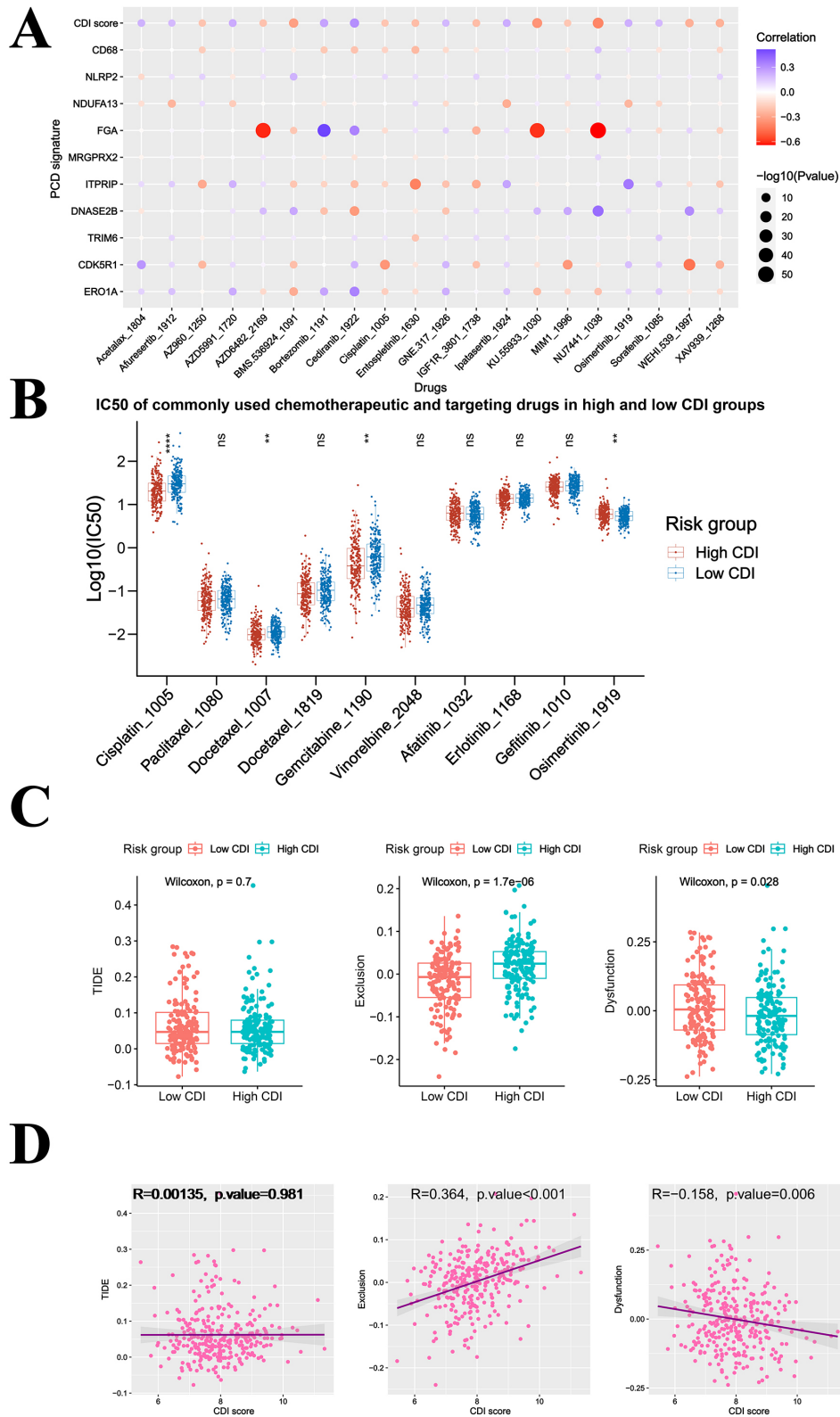


Fig. 8. Prediction of CDI-Related Drug Sensitivity. (A) Bubble plot demonstrating the correlation prediction between CDI score, CDI genes, and sensitivity to various anticancer drugs in LUAD patients from TCGA, with bubble colors indicating the level of correlation and bubble size representing statistical significance. (B) Box plots presenting IC50 values for common chemotherapy and targeted drugs in high CDI and low CDI groups. (C) Box plots showing TIDE score, Exclusion score, and Dysfunction score in high CDI and low CDI groups. (D) Scatter plots describing the correlation between CDI score and Tumor Immune Dysfunction and Exclusion (TIDE) score, Exclusion score, and Dysfunction score. **, $p < 0.01$; ***, $p < 0.0001$; ns, non-significant.

apoptosis correlates with unfavorable survival outcomes in LUAD patients. This association may be explained by the non-immunogenic consequences of apoptosis.

Two autophagy genes, *CDK5R1* and *TRIM6*, stand out as significant independent risk factors in the prognostic model, each with HRs >1 and *p* values < 0.01, indicating that autophagy might play a relatively critical role in the cell death profile of LUAD. *CDK5R1*, or Cyclin-Dependent Kinase 5 Regulatory Subunit 1, serves as a subunit of *CDK5* (Cyclin-Dependent Kinase 5). *CDK5* exerts diverse biological effects by phosphorylating various regulatory substrates. The functionality of *CDK5* is intimately associated with autophagy, and animal models lacking *CDK5* functionality exhibit reduced autophagy occurrence and shortened lifespan [20]. The tumor microenvironment has long been recognized as a nutrient-depleted setting, while autophagy acting as a surviving process adopted by eukaryotic cells in response to nutrient stress circumstances [21]. The fusion of autophagosome with lysosome can thus supply an additional energy support. Tumor cells can also undergo autophagy process which might inhibit cytokine-mediated apoptosis and thus avoid T cell-induced cytotoxicity [22]. The suppression of tumor cell autophagy has the potential to promote tumor cell clearance within the tumor microenvironment [23]. Furthermore, autophagy has the capacity to interact with various types of PCD such as apoptosis, thereby collectively influencing tumor metastasis and anti-cancer immune reactions [11,24].

Pyroptosis, similar to necroptosis, represents an immunogenic cell death program characterized by plasma membrane perforation, subsequently leading to the release of pro-inflammatory cellular contents [25]. Pyroptosis in the tumor microenvironment can result in the release of proinflammatory cytokines such as IL-1 β , IL-18 to enable the infiltration of immunocytes into the tumor microenvironment, indicating that pyroptosis could be developed in anti-cancer treatment [26]. Employing a biorthogonal strategy to elucidate the pyroptotic processes in live organisms, it was determined that a proportion of 15% of tumor cells undergoing pyroptosis could potentiate T cell response, ultimately contributing to the complete remission of solid tumor [27]. Pyroptosis can also be activated by specific nanoparticles, thereby promoting anti-cancer immunity through stimulating effector-memory T cells and inhibiting cancer cell proliferation and invasion [28,29]. The present study reveals that the pyroptosis gene *NLRP2* is an independent protective factor (Hazard Ratio (HR) = 0.893, *p* = 0.0019), indicating that the pyroptosis process is related with a higher probability of survival. *NLRP2* is characterized by an N-terminal pyrin domain and is implicated in the activation of caspase-1 through Toll-like receptors. Additionally, it participates in protein complexes that trigger proinflammatory caspases, crucially contributing to the pyroptosis process. Several studies investigating pyroptosis or genes associated with pyroptosis have demonstrated a

significant correlation between *NLRP2* and both pyroptosis and disease prognosis [30]. Other investigations have indicated that *NLRP2* is positively associated with survival rates, while exhibiting a negative correlation with cancer metastasis [31]. Gain- and loss-of-function studies conducted *in vitro* and *in vivo* have revealed that the overexpression of *NLRP2* significantly inhibits the growth and metastasis of breast cancer cells in xenograft models. Furthermore, *NLRP2* enhances the H₂O₂-induced elevation of p53 and Bax, consequently leading to a substantial increase in the rate of apoptosis. Moreover, *NLRP2* facilitates the nuclear entry of p53, promoting apoptosis. These findings collectively suggest that *NLRP2* may play a pivotal role in the biological responses of tumors, particularly in the pyroptosis process.

Despite that the prognostic model exhibited good performance in both the internal and external database, there are several limitations. For instance, the patients included in the study were retrospectively enrolled, which might result in unavoidable bias. Besides, there is limited clinical trials to clarify the value of the prognostic PCD model in decision-making of patient selection who might be sensitive to specific treatment such as EGFR-TKI.

5. Conclusions

In conclusion, the PCD gene signature identified in the current research holds practical utility for prognostic prediction and evaluation of the immune status for LUAD patients. The gene patterns of twelve programmed cell death might provide insights into deeper mechanism and offer potential novel targets for lung cancer treatment.

Availability of Data and Materials

All data generated or analysed during this study are included in this published article and its supplementary information files.

Author Contributions

(I) Conception and design: FC, JM and JL. (II) Administrative support: FC, SH and JL. (III) Provision of study materials or patients: FC, CW and SC. (IV) Collection and assembly of data: FC, SH, JM and CW. (V) Data analysis and interpretation: All authors. (VI) Drafting the work or reviewing it critically for important intellectual content: All authors. (VII) Final approval of the version to be published: All authors. (VIII) All authors agreed to be accountable for all aspects of the work in ensuring that questions related to the accuracy or integrity of any part of the work are appropriately investigated and resolved.

Ethics Approval and Consent to Participate

Not applicable.

Acknowledgment

Not applicable.

Funding

This research received no external funding.

Conflict of Interest

The authors declare no conflict of interest.

Supplementary Material

Supplementary material associated with this article can be found, in the online version, at <https://doi.org/10.31083/j.fbl2904135>.

References

- [1] Sung H, Ferlay J, Siegel RL, Laversanne M, Soerjomataram I, Jemal A, *et al.* Global Cancer Statistics 2020: GLOBOCAN Estimates of Incidence and Mortality Worldwide for 36 Cancers in 185 Countries. *CA: a Cancer Journal for Clinicians*. 2021; 71: 209–249.
- [2] Siegel RL, Miller KD, Wagle NS, Jemal A. Cancer statistics, 2023. *CA: a Cancer Journal for Clinicians*. 2023; 73: 17–48.
- [3] Mao Y, Yang D, He J, Krasna MJ. Epidemiology of Lung Cancer. *Surgical Oncology Clinics of North America*. 2016; 25: 439–445.
- [4] Howlader N, Forjaz G, Mooradian MJ, Meza R, Kong CY, Cronin KA, *et al.* The Effect of Advances in Lung-Cancer Treatment on Population Mortality. *The New England Journal of Medicine*. 2020; 383: 640–649.
- [5] DeSantis CE, Miller KD, Goding Sauer A, Jemal A, Siegel RL. Cancer statistics for African Americans, 2019. *CA: a Cancer Journal for Clinicians*. 2019; 69: 211–233.
- [6] Vanden Berghe T, Linkermann A, Jouan-Lanhouet S, Walczak H, Vandenabeele P. Regulated necrosis: the expanding network of non-apoptotic cell death pathways. *Nature Reviews. Molecular Cell Biology*. 2014; 15: 135–147.
- [7] Shi Z, Yuan S, Shi L, Li J, Ning G, Kong X, *et al.* Programmed cell death in spinal cord injury pathogenesis and therapy. *Cell Proliferation*. 2021; 54: e12992.
- [8] Galluzzi L, Vitale I, Aaronson SA, Abrams JM, Adam D, Agostinis P, *et al.* Molecular mechanisms of cell death: recommendations of the Nomenclature Committee on Cell Death 2018. *Cell Death and Differentiation*. 2018; 25: 486–541.
- [9] Tang D, Kang R, Berghe TV, Vandenabeele P, Kroemer G. The molecular machinery of regulated cell death. *Cell Research*. 2019; 29: 347–364.
- [10] Zhang T, Wu DM, Luo PW, Liu T, Han R, Deng SH, *et al.* CircNEIL3 mediates pyroptosis to influence lung adenocarcinoma radiotherapy by upregulating PIF1 through miR-1184 inhibition. *Cell Death & Disease*. 2022; 13: 167.
- [11] Su Z, Yang Z, Xu Y, Chen Y, Yu Q. Apoptosis, autophagy, necroptosis, and cancer metastasis. *Molecular Cancer*. 2015; 14: 48.
- [12] Xie X, Wang J, Shi D, Zou Y, Xiong Z, Li X, *et al.* Identification of a 4-mRNA metastasis-related prognostic signature for patients with breast cancer. *Journal of Cellular and Molecular Medicine*. 2019; 23: 1439–1447.
- [13] Herdiana Y, Sriwidodo S, Sofian FF, Wilar G, Diantini A. Nanoparticle-Based Antioxidants in Stress Signaling and Programmed Cell Death in Breast Cancer Treatment. *Molecules (Basel, Switzerland)*. 2023; 28: 5305.
- [14] Chen J, Ye M, Bai J, Hu C, Lu F, Gu D, *et al.* Novel insights into the interplay between m6A modification and programmed cell death in cancer. *International Journal of Biological Sciences*. 2023; 19: 1748–1763.
- [15] Jang JY, Im E, Choi YH, Kim ND. Mechanism of Bile Acid-Induced Programmed Cell Death and Drug Discovery against Cancer: A Review. *International Journal of Molecular Sciences*. 2022; 23: 7184.
- [16] Green DR, Ferguson T, Zitvogel L, Kroemer G. Immunogenic and tolerogenic cell death. *Nature Reviews. Immunology*. 2009; 9: 353–363.
- [17] Taylor RC, Cullen SP, Martin SJ. Apoptosis: controlled demolition at the cellular level. *Nature Reviews. Molecular Cell Biology*. 2008; 9: 231–241.
- [18] Li G, Mongillo M, Chin KT, Harding H, Ron D, Marks AR, *et al.* Role of ERO1- α -mediated stimulation of inositol 1,4,5-triphosphate receptor activity in endoplasmic reticulum stress-induced apoptosis. *The Journal of Cell Biology*. 2009; 186: 783–792.
- [19] Ellis HM, Horvitz HR. Genetic control of programmed cell death in the nematode *C. elegans*. *Cell*. 1986; 44: 817–829.
- [20] Nandi N, Krämer H. Cdk5-mediated Acn/Acinus phosphorylation regulates basal autophagy independently of metabolic stress. *Autophagy*. 2018; 14: 1271–1272.
- [21] Harnett MM, Pineda MA, Latré de Laté P, Eason RJ, Besteiro S, Harnett W, *et al.* From Christian de Duve to Yoshinori Ohsumi: More to autophagy than just dining at home. *Biomedical Journal*. 2017; 40: 9–22.
- [22] Young TM, Reyes C, Pasnikowski E, Castanaro C, Wong C, Decker CE, *et al.* Autophagy protects tumors from T cell-mediated cytotoxicity via inhibition of TNF α -induced apoptosis. *Science Immunology*. 2020; 5: eabb9561.
- [23] Pellegrini P, Strambi A, Zipoli C, Hägg-Olofsson M, Buoncervello M, Linder S, *et al.* Acidic extracellular pH neutralizes the autophagy-inhibiting activity of chloroquine: implications for cancer therapies. *Autophagy*. 2014; 10: 562–571.
- [24] Mukhopadhyay S, Panda PK, Sinha N, Das DN, Bhutia SK. Autophagy and apoptosis: where do they meet? *Apoptosis: an International Journal on Programmed Cell Death*. 2014; 19: 555–566.
- [25] Fink SL, Cookson BT. Apoptosis, pyroptosis, and necrosis: mechanistic description of dead and dying eukaryotic cells. *Infection and Immunity*. 2005; 73: 1907–1916.
- [26] Tan Y, Chen Q, Li X, Zeng Z, Xiong W, Li G, *et al.* Pyroptosis: a new paradigm of cell death for fighting against cancer. *Journal of Experimental & Clinical Cancer Research: CR*. 2021; 40: 153.
- [27] Wang Q, Wang Y, Ding J, Wang C, Zhou X, Gao W, *et al.* A bioorthogonal system reveals antitumor immune function of pyroptosis. *Nature*. 2020; 579: 421–426.
- [28] Ding B, Sheng J, Zheng P, Li C, Li D, Cheng Z, *et al.* Biodegradable Upconversion Nanoparticles Induce Pyroptosis for Cancer Immunotherapy. *Nano Letters*. 2021; 21: 8281–8289.
- [29] Zhao P, Wang M, Chen M, Chen Z, Peng X, Zhou F, *et al.* Programming cell pyroptosis with biomimetic nanoparticles for solid tumor immunotherapy. *Biomaterials*. 2020; 254: 120142.
- [30] Chen L, Shi C, Zhou G, Yang X, Xiong Z, Ma X, *et al.* Genome-wide exploration of a pyroptosis-related gene module along with immune cell infiltration patterns in bronchopulmonary dysplasia. *Frontiers in Genetics*. 2023; 13: 1074723.
- [31] Yan C, Niu Y, Li F, Zhao W, Ma L. System analysis based on the pyroptosis-related genes identifies GSDMC as a novel therapy target for pancreatic adenocarcinoma. *Journal of Translational Medicine*. 2022; 20: 455.